First optimization steps for the Nanocluster Synthesis of Platinum-Yttrium Alloys: Insights from a sputter gas aggregation source

M. Fenker[1], L.-M. Weinhold[1,2], J. Albrecht[2] and H. Kaßner[1]

[1]*fem Forschungsinstitut, Katharinenstraße 13-17, 73525 Schwäbisch Gmünd, Germany*
[2]*Research Institute for Innovative Surfaces FINO, Aalen University, Aalen, Germany*

(Received: 02. Dec. 2024, Accepted: 27. Dec. 2024, Published online: 30. Dec. 2024)

Nanoclusters (NCs) are critical in advanced technologies due to their unique size-dependent properties, offering significant potential in catalysis, energy storage, energy conversion and electronic devices. In this study, the first steps were taken towards optimizing the synthesis of nanoclusters from platinum-yttrium alloys for cost-efficient fuel cell technologies, employing a magnetron sputtering system combined with a gas aggregation source. Copper was used as a benchmark material to investigate the effects of varying gas flow rates, aggregation lengths, and coating times on cluster size. Subsequently, experiments with yttrium and platinum were conducted. NC sizes in the range of 4 to 12 nm could be synthesized. These results provide a comprehensive parameter map for NC synthesis and contribute to the further development of this kind of synthesis for sustainable fuel cell technology by reducing platinum consumption and improving catalytic efficiency.

(DOI: 10.31281/sw4j0v67)

fenker@fem-online.de

I. Introduction

In recent years, nanoclusters (NCs) and nanoparticles (NPs) have emerged as key materials in various technological applications due to their unique size-dependent properties and the tunability of their chemical and physical characteristics. These materials are increasingly employed in fields ranging from catalysis, energy storage and energy conversion to biomedicine and advanced electronic devices [1,2]. Among the synthesis techniques, gas-phase methods, particularly those based on magnetron sputtering and gas aggregation sources, have gained prominence for their ability to produce ultra-pure NPs with controlled size and composition [3,4]. A system that combines sputtering and gas-phase aggregation for nanoparticle synthesis is called sputter gas aggregation source (SGAS) [3,5–7]. The fundamental mechanism for the formation of nanoclusters using the SGAS technique is gas condensation within the aggregation zone of the nanocluster source.

The development of advanced SGAS techniques, including the Multiple Ion Cluster Source (MICS), represents a significant leap forward, enabling the fabrication of complex core@shell structures, alloy NPs, and precisely size-selected clusters. These innovations allow the integration of functionality and versatility into NPs, overcoming many of the limitations inherent in chemical synthesis methods [8,9]. For example, MICS technology has facilitated the scalable production of NPs with tailored chemical compositions while maintaining stringent control over particle purity and size distribution [4,10].

Despite their remarkable potential, challenges persist in optimizing synthesis techniques for industrial-scale production and in achieving long-term operational stability. Addressing these issues is crucial for expanding the applicability of NPs in high-tech applications such as non-volatile

memory devices, photonics, and energy conversion systems [11,12]. Recent studies have demonstrated promising solutions, such as integrating in situ characterization tools and employing modular systems for enhanced control during NP synthesis [10,13].

This study focuses on addressing the challenges associated with reducing the platinum content in fuel cell technology to lower production costs and mitigate CO_2 emissions. platinum-yttrium alloy nanoclusters (NCs) are proposed as a promising alternative due to their high catalytic activity and large active surface area [14–18]. In the frame of this work, initial parameter studies were conducted using a nanocluster source, which employs a magnetron sputtering system (i.e. a SGAS system) for NC generation. Starting with copper as a benchmark material, variations in coating time, gas inlet location, gas flow, and aggregation length were systematically explored. Subsequent experiments with yttrium revealed the need for higher magnetron power, which led to significant heat input and reduced cluster sizes. Finally, platinum clusters were generated through gas flow and aggregation length variations. These findings provide a foundational understanding of the parameter space for optimizing nanocluster synthesis and contribute to advancing cost-efficient fuel cell technologies.

II. Methods/Experimental Setup

II.a) Experimental setup

For the nanocluster deposition studies, a nanocluster source (NC200 U-B, Oxford Applied Research, UK) was flanged to an existing vacuum system (Cobra Cube, CCR GmbH, Germany) (see photo in Figure 1). The core of the nanocluster source is a water-cooled magnetron sputter source with a target size of 50.8 mm. The target materials copper, yttrium and platinum were used for the experiments with the nanocluster source. The maximum power is 1000 W, and the applied voltage should be in the range from 4 V to 500 V. A pulsed DC generator ENI RPG-50 (MKS-ENI, Germany) was used as the power supply. Table 1 shows the most important process parameters for the investigations carried out in this work. A schematic representation and detailed description of the nanocluster source can be found in the publications [10] and [11]. The water-cooled aggregation zone is connected to the outer stainless steel tube and the coating chamber of the Cobra Cube through an opening. The size of the opening can be adjusted using a nozzle and aperture plate. The working gas argon can be introduced at two different locations independently of each other: a) at the sputter source and b) at the aggregation zone.

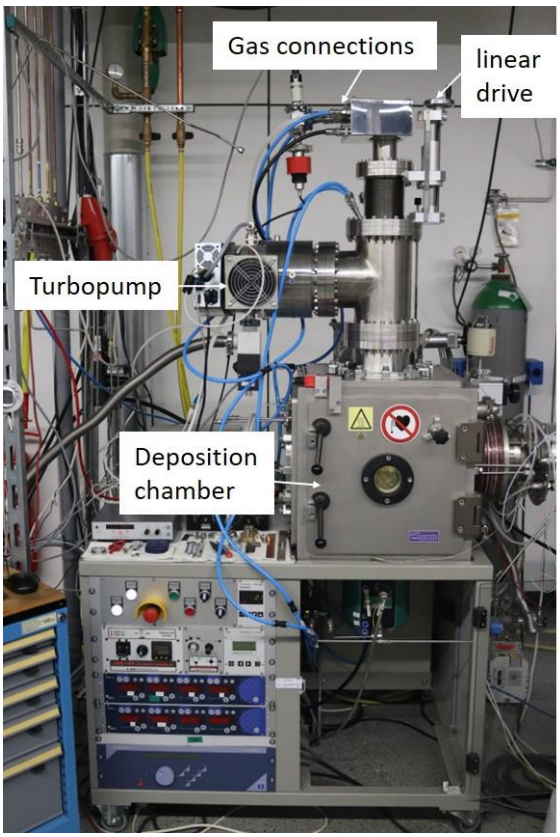

Figure 1: Photo of the nanocluster source on top of the vacuum vessel, i.e. the deposition chamber. The linear drive is for moving the sputtering source, to change the aggregation length.

First, two coating experiments were carried out on silicon samples to determine the influence of the inlet location of the working gas. The results suggested that the formation of the coating and nanoclusters is largely independent of the type of gas inlet used, as no differences were observable through optical inspection. Therefore, a fixed Ar gas flow rate of 9 sccm was set at the aggregation zone for the subsequent tests and no further variations were made. The variation of the Ar gas flow rate was thus carried out at the sputter source.

A substrate holder was manufactured and positioned directly below the orifice of the nanocluster source, but inside the deposition chamber. Silicon wafers and TEM grids (STEM investigations) were used as substrate materials for studies.

Process parameter	Unit	Cu	Y	Pt
Target power	W	65-70	244	60
Discharge current	mA	200	1200	200
Discharge voltage	V	300-330	204	300
Ar gas flow rate	sccm	12…80	12	16…90
Aggregation length	mm	40, 90, 140	140	40, 90, 140
Sputtering Yield [19] (Ar, E_{ion}= 500 eV)	-	2.4	0.7	1.45

Table 1: Process parameters for the deposition of Cu, Y and Pt nanoclusters with a SGAS and the sputtering yield of these target materials.

II.b) Characterisations

The size and composition of the nanoclusters were characterized using a Zeiss field emission scanning electron microscope (FE-SEM), model Gemini EM 300. The Transmission Electron Microscope (TEM) grids are characterized using the Scanning Transmission Electron Microscope (STEM) mode of the Auriga 60 field emission scanning electron microscope from Zeiss. The IMS Client image processing program from Imagic was used to evaluate the cluster size. The thickness of the porous coating of the nanocluster deposition was detected using the usurf custom confocal microscope from Nanofocus.

III. Results

This paragraph is divided into three subsections. In these three subsections, the results of the investigations of the deposition of Cu, Y and Pt nanoclusters are presented.

Before these subsections begin, the influence of the argon gas flow on the pressure in the aggregation zone should be briefly discussed, as this result is relevant for all three subsections. Figure 2 shows the dependence of the pressure on the set argon gas flow rate. As the gas flow increases, the pressure in the aggregation zone rises. As can be seen from Figure 2, the curve is basically linear. Only in the range 16 to 50 sccm does the curve deviate slightly from linearity. Overall, pressures in the sub-Pascal range are achieved (approximately 0.1 to 0.6 Pa).

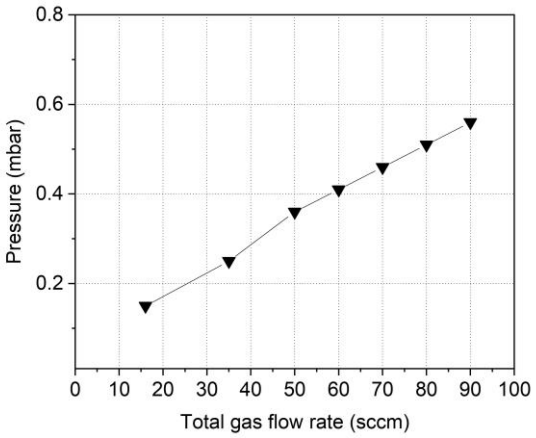

Figure 2: Graph visualizing the pressure in the aggregation zone as a function of the total gas flow.

III.a) Copper nanocluster

In the experiments with a copper target mounted in the nanocluster source, the coating time, the gas inlet position, the gas flow rate and the aggregation length were varied.

For the first depositions the coating time was changed from 30 s to 240 s. It was found that the nanoclusters agglomerate and form a kind of porous coating (see figure 1). The growth rate for this porous coating is approx. 70 µm/h. However, mono-cluster layers are required for use as catalytic material for fuel cells, as these are more

material and therefore cost-efficient. Therefore, only coating times of a few seconds were selected for further investigations.

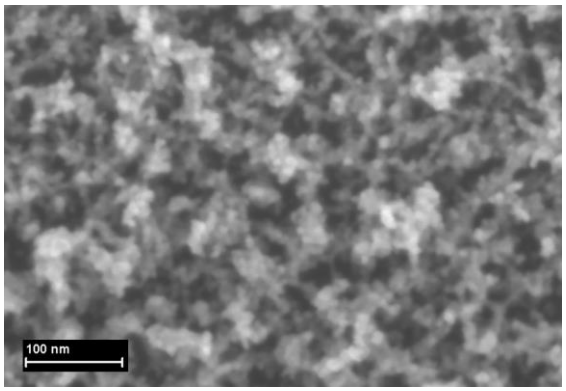

Figure 3: SEM image of a Cu porous coating at 200,000x magnification with an aggregation length of 140 mm and 14 sccm Ar flow rate.

The nanocluster size can be influenced by changing the gas flow rate. In Figure 4 the relationship between gas flow rate and copper cluster size is illustrated. At low flow rates (12–23 sccm), cluster sizes are small (around 6 nm) with minimal variability. As the flow rate increases to 50 and 80 sccm, the cluster size grows significantly to about 11 nm, accompanied by greater variability in size. The sharp increase in cluster size occurs between 23 and 50 sccm, while sizes stabilize at higher flow rates. These results suggest that higher gas flow rates promote the formation of larger, but less uniform, clusters.

To get an impression of the size and distribution of the Cu nanoclusters, three selected STEM images are shown in Figure 6. The change from small nanoclusters (at 12 sccm) to large ones (at 50 and 80 sccm) is clearly visible. However, agglomeration of the nanoclusters already occurs at the higher gas flow rates, so that the increased size distribution is not easily recognizable.

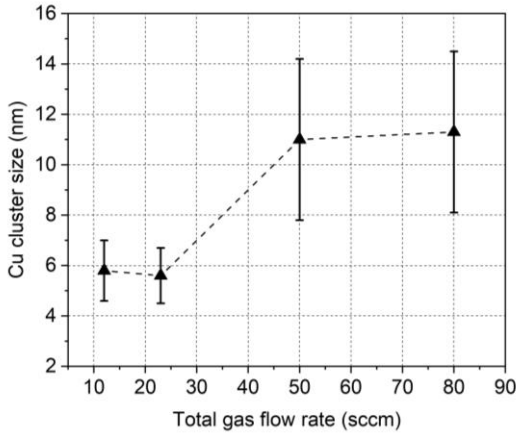

Figure 4: Relationship between total gas flow rate and cluster size of copper NCs with an aggregation length of 140 mm. The error bars represent the standard deviation of the measurements.

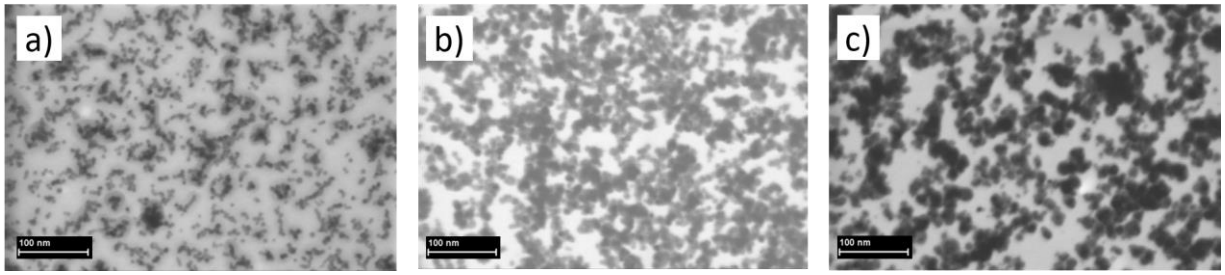

Figure 5: STEM images (magnification 200,000x) of copper nanoclusters with variations of the gas flows at an aggregation length of 140 mm, with gas flow rates of a) 12 sccm, b) 50 sccm, and c) 80 sccm.

Cu nanoclusters were also deposited at different aggregation lengths and analysed by STEM. The measured copper nanocluster sizes are shown in Table 2 together with a variation of the gas flow rate.

No significant size difference was observed between aggregation lengths of 140 mm and 90 mm across the entire gas flow range. The largest size increase (55.0%) was measured between gas flows of 14 sccm and 50 sccm at 140 mm, while the difference between 50 sccm and 80 sccm (3.7%) was negligible. Significantly smaller cluster sizes were found for an aggregation length of 40 mm. When the Ar gas flow rate is varied, a maximum is formed here at approx. 50 sccm. This was not measured for the other two aggregation lengths.

Aggr. Length (mm)	Ar gas flow rate (sccm)		
	14	50	80
140	6.2±1.6	10.9±3.2	11.3±3.2
90	6.9±2.0	10.6±3.3	12.1±5.7
40	4.8±1.6	8.2±1.7	6.4±1.2

Table 2: Cu cluster sizes (in nanometres) as a function of aggregation length and Ar gas flow rate.

Thus, Cu nanoclusters with a size of 5 to 12 nm could be deposited in the investigated parameter space.

III.b) Yttrium nanocluster

The deposition of yttrium nanoclusters requires significantly higher power (~240 W), approximately four times that needed for copper cluster deposition. The reason for this is the 3.4-fold lower sputtering yield of yttrium compared to Cu Table 1. These high power levels cause a substantial temperature increase in the aggregation zone during extended operation, though the temperature cannot be directly measured due to system limitations. To approximate conditions, the temperature of the cooling water in the return flow was recorded using a thermocouple attached to the aggregation zone's pipe. Starting at 18°C, the cooling water temperature rose to 40°C after 11 minutes of sputtering at 244 W, and further increased to 58°C after deposition. It is assumed that the aggregation zone's temperature is considerably higher. Additionally, the power and voltage were unstable throughout the deposition process.

The nanoclusters were analysed at 20,000x magnification by STEM. The cluster size from the "cold" system was measured at 20.2 ± 6.3 nm (see Figure 6), while the "hot" system produced clusters of 12.8 ± 3.3 nm. This demonstrates that both the applied power and the resulting system heating significantly influence cluster size. Maintaining consistent temperatures is therefore critical for comparative studies.

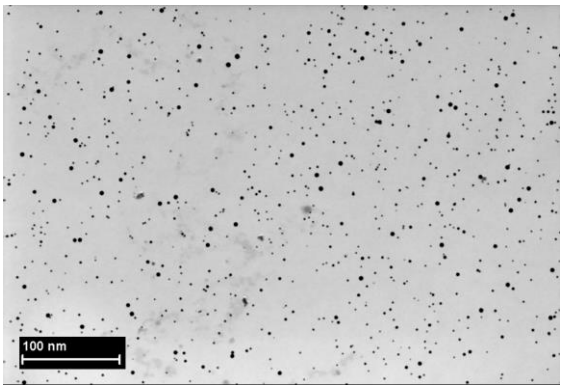

Figure 6: STEM images of yttrium clusters at 20,000x magnification with the vacuum system in the cold state and with an aggregation length of 140 mm and 12 sccm Ar flow rate.

Due to the impact of heating on cluster size, experiments on yttrium cluster deposition were not further pursued in this study. Cooling the aggregation zone solely with water proved insufficient for the power range and prolonged deposition times required for yttrium. As an alternative for future work, a platinum target coated with yttrium foil strips could be used for the intended Pt_xY alloy, as reported by Lindahl et al. [16].

III.c) Platinum nanocluster

In the experiments with a platinum target, the gas flow rate and the aggregation length were varied.

Figure 7 shows the relationship between the argon gas flow rate and the cluster size of platinum NCs. The curve reveals a distinct trend: an initial increase in cluster size as the gas flow rate rises, reaching a maximum cluster size of approximately 8 nm at a gas flow rate of 50 sccm. Beyond this point, the cluster size declines steadily, indicating an inverse relationship between gas flow and cluster formation at higher flow rates. The observed error bars become wider at certain flow rates, suggesting greater variability in cluster sizes at these conditions.

This behavior may be associated with the dynamics of gas-particle interactions during the clustering process. At lower gas flows, increased residence times might favor larger cluster formation. With further increase of the gas flow the excess Ar-gas does not contribute to the sputtering process and flows away quickly through the aggregation zone. This process helps the cluster to have shorter residence time in the aggregation zone or to leave the aggregation zone relatively faster, which restricts the growth of the clusters bigger in sizes [10].

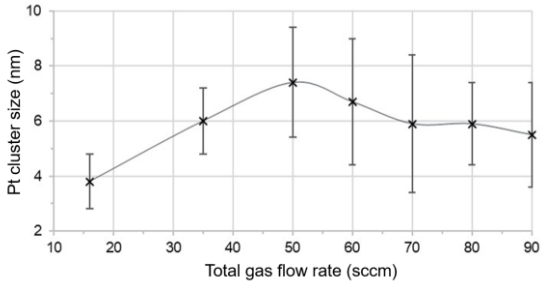

Figure 7: Relationship between total gas flow rate and cluster size of platinum NCs with an aggregation length of 140 mm. The error bars represent the standard deviation of the measurements.

A comparison of the "cluster size-total gas flow rate" curves of Pt NCs (Figure 7) with those of Cu NCs (Figure 4) shows that the synthesis of NCs for the two metals react differently to the variation of the gas flow rate. The discharge parameters of Cu and Pt are practically identical (see Table 1). However, there is an obvious difference in the higher sputtering yield of Cu (2.4) compared to Pt (1.45). Further differences can be assumed in the interaction of the sputtered metals with the Ar gas, as well as in the gas phase condensation of the metals.

To get an impression of the size and distribution of the Pt nanoclusters, three selected STEM images are shown in Figure 8. As can be observed, at the lowest flow rate the nanoclusters are very small (approx. 4 nm) and have a similar size. At the higher flow rates, a broader distribution of nanocluster size can be recognized. Furthermore, the number of nanoclusters is significantly lower than at the Ar flow rate of 16 sccm.

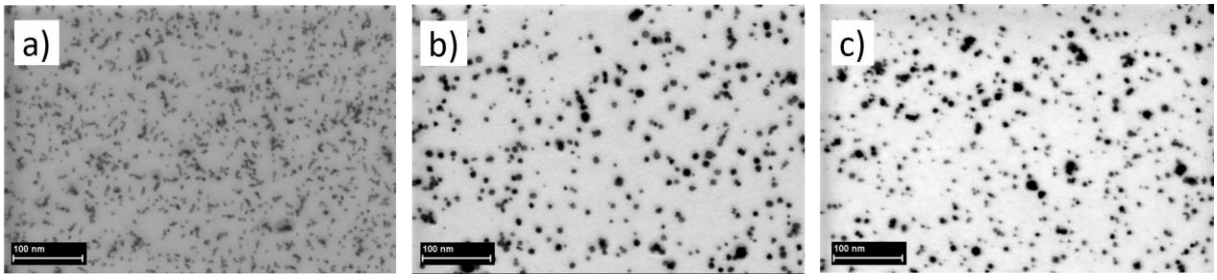

Figure 8: STEM images (magnification 200,000x) of platinum nanoclusters with variations of the gas flows at an aggregation length of 140 mm, with gas flow rates of a) 16 sccm, b) 50 sccm, and c) 80 sccm.

For platinum, a comparison of the influence of the aggregation length and the Ar gas flow rate on the cluster size is listed in Table 3. The cluster sizes were evaluated using STEM images taken at a magnification of 200,000x. It can be recognised that over the entire gas flow range the result from subsection III.a) for the synthesis of Cu NCs could be confirmed. The change in length of the aggregation zone does not result in any recognizable change in the cluster sizes of platinum. What is also noticeable (not shown here) is the high density of nanoclusters with a low aggregation length at higher gas flows.

Aggr. Length (mm)	Ar gas flow rate (sccm)		
	16	50	80
140	3.8±1.0	7.4±2.0	5.8±1.5
90	4.2±0.8	6.6±1.6	5.3±2.1
40	3.1±0.8	5.3±1.2	5.9±1.3

Table 3: Pt cluster sizes (in nanometres) as a function of aggregation length and Ar gas flow rate.

IV. Conclusions

In this work, Cu, Y and Pt NCs were deposited using a sputter gas aggregation source (SGAS). The study highlights the critical role of process parameters, such as gas flow rate, aggregation

length, target power and power stability, in the synthesis of nanoclusters. The following cluster sizes could be synthesized in the parameter space examined:

- Cu NCs: 5-12 nm
- Y NCs: 13-20 nm
- Pt NCs: 3-7 nm

A larger cluster size would be desirable for the synthesis of Pt NCs. Increasing the target power could deliver an improvement here in the future. The findings also underline the importance of thermal management during yttrium deposition and the necessity of achieving stable operating conditions for consistent cluster size. Future work will focus on enhancing the scalability of this technique and further refining NC size control for broader industrial applications, including energy storage and catalysis.

V. Acknowledgements

The IGF project 01IF22772 N "VAPtYL" of the research association Edelmetalle und Metallchemie is funded by the Federal Ministry for Economic Affairs and Climate Action (BMWK) via the DLR as part of the program for the promotion of joint industrial research (IGF) on the basis of a resolution of the German Bundestag. Furthermore, we would like to thank the following colleagues of the fem Forschungsinstitut: a) for SEM/STEM investigations: R. Bretzler and B. Schöne, b) for support in the implementation of the nanocluster source into the vacuum system: M. Balzer and K. Petrikowski.

VI. References

[1] A. Majumdar, D. Köpp, M. Ganeva, D. Datta, S. Bhattacharyya, R. Hippler, Development of metal nanocluster ion source based on dc magnetron plasma sputtering at room temperature, *Rev. Sci. Instrum.* 80 (2009) 095103. https://doi.org/10.1063/1.3213612.

[2] D. Llamosa, M. Ruano, L. Martínez, A. Mayoral, E. Roman, M. García-Hernández, Y. Huttel, The ultimate step towards a tailored engineering of core@shell and core@shell@shell nanoparticles, Nanoscale 6 (2014) 13483–13486. https://doi.org/10.1039/C4NR02913E.

[3] Y. Huttel, L. Martínez, A. Mayoral, I. Fernández, Gas-phase synthesis of nanoparticles: present status and perspectives, *MRS Commun.* 8 (2018) 947–954. https://doi.org/10.1557/mrc.2018.169.

[4] L. Martínez, K. Lauwaet, G. Santoro, J.M. Sobrado, R.J. Peláez, V.J. Herrero, I. Tanarro, G.J. Ellis, J. Cernicharo, C. Joblin, Y. Huttel, J.A. Martín-Gago, Precisely controlled fabrication, manipulation and in-situ analysis of Cu based nanoparticles, *Sci. Rep.* 8 (2018) 7250. https://doi.org/10.1038/s41598-018-25472-y.

[5] J.A. De Toro, P.S. Normile, C. Binns, Types of Cluster Sources, in: *Gas-Phase Synth. Nanoparticles*, John Wiley & Sons, Ltd, 2017: pp. 39–55. https://doi.org/10.1002/9783527698417.ch3.

[6] M. Khojasteh, V.V. Kresin, Influence of source parameters on the growth of metal nanoparticles by sputter-gas-aggregation, *Appl. Nanosci.* 7 (2017) 875–883. https://doi.org/10.1007/s13204-017-0627-2.

[7] M. Khojasteh, Fabrication, deposition, and characterization of size-selected metal nanoclusters with a magnetron sputtering gas aggregation source, *PhD thesis*, Faculty of the Graduate School University of Southern California, 2019.

[8] D. Llamosa Perez, L. Martínez, Y. Huttel, Multiple Ion Cluster Source for the Generation of Magnetic Nanoparticles: Investigation of the Efficiency as a Function of the Working Parameters for the Case of Cobalt, Dataset Pap. Sci. 2014 (2014) 584391. https://doi.org/10.1155/2014/584391.

[9] L. Martínez, A. Mayoral, M. Espiñeira, E. Roman, F.J. Palomares, Y. Huttel, Core@shell, Au@TiO_x nanoparticles by gas phase synthesis, Nanoscale 9 (2017) 6463–6470. https://doi.org/10.1039/C7NR01148B.

[10] S. Mondal, S.R. Bhattacharyya, Performance of a size-selected nanocluster deposition facility and *in situ* characterization of grown films by x-ray photoelectron spectroscopy, *Rev. Sci. Instrum.* 85 (2014) 065109. https://doi.org/10.1063/1.4882315.

[11] D. Biswas, S. Mondal, A. Rakshit, A. Bose, S. Bhattacharyya, S. Chakraborty, Size and density controlled Ag nanocluster embedded MOS structure for memory applications, *Mater. Sci. Semicond. Process.* 63 (2017) 1–5. https://doi.org/10.1016/j.mssp.2017.01.015.

[12] S.G. Praveen, C. Bansal, D.J. Nagar, Inter-cluster separation induced change in charge transport mechanism in Ni40Pd60 nanoclusters, *Sci. Rep.* 9 (2019) 7513. https://doi.org/10.1038/s41598-019-43581-0.

[13] Y. Huttel, O.L. Martínez, M.I. Fernández, Vorrichtung Und Verfahren Zur Stabilen Herstellung Von Nanoclustern, EP3605583A1, 2020.

[14] J. Greeley, I.E.L. Stephens, A.S. Bondarenko, T.P. Johansson, H.A. Hansen, T.F. Jaramillo, J. Rossmeisl, I. Chorkendorff, J.K. Nørskov, Alloys of platinum and early transition metals as oxygen reduction electrocatalysts, *Nat. Chem.* 1 (2009) 552–556. https://doi.org/10.1038/nchem.367.

[15] I.E.L. Stephens, A.S. Bondarenko, L. Bech, I. Chorkendorff, Oxygen Electroreduction Activity and X-Ray Photoelectron Spectroscopy of Platinum and Early Transition Metal Alloys, *ChemCatChem* 4 (2012) 341–349. https://doi.org/10.1002/cctc.201100343.

[16] N. Lindahl, E. Zamburlini, L. Feng, H. Grönbeck, M. Escudero-Escribano, I.E.L. Stephens, I. Chorkendorff, C. Langhammer, B. Wickman, High Specific and Mass Activity for the Oxygen Reduction Reaction for Thin Film Catalysts of Sputtered Pt_3 Y, *Adv. Mater. Interfaces* 4 (2017) 1700311. https://doi.org/10.1002/admi.201700311.

[17] H.L. Brown, S.A. Thornley, S.J. Wakeham, M.J. Thwaites, R.J. Curry, M.A. Baker, The impact of substrate bias on a remote plasma sputter coating process for conformal coverage of trenches and 3D structures, *J. Phys. Appl. Phys.* 48 (2015) 335303. https://doi.org/10.1088/0022-3727/48/33/335303.

[18] B. Eriksson, G. Montserrat-Sisó, R. Brown, T. Skála, R. Wreland Lindström, G. Lindbergh, B. Wickman, C. Lagergren, Enhanced oxygen reduction activity with rare earth metal alloy catalysts in proton exchange membrane fuel cells, *Electrochimica Acta* 387 (2021) 138454. https://doi.org/10.1016/j.electacta.2021.138454.

[19] Y. Yamamura, H. Tawara, ENERGY DEPENDENCE OF ION-INDUCED SPUTTERING YIELDS FROM MONATOMIC SOLIDS AT NORMAL INCIDENCE, *At. Data Nucl. Data Tables* 62 (1996) 149–253. https://doi.org/10.1006/adnd.1996.0005.